NASA TECHNICAL NOTE

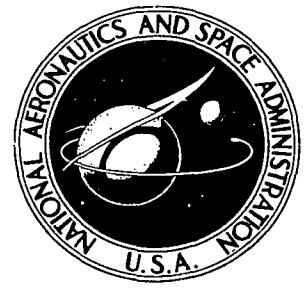

NASA TN D-6592

NASA TN D-6592

MIXING OF SUPERSONIC JETS INCLUDING THE EFFECTS OF TRANSVERSE PRESSURE GRADIENT USING DIFFERENCE METHODS

by Anatole P. Kurkov

Lewis Research Center
Cleveland, Ohio 44135

NATIONAL AERONAUTICS AND SPACE ADMINISTRATION • WASHINGTON, D. C. • DECEMBER 1971

1. Report No.	2. Government Accession No.	
NASA TN D-6592		

4. Title and Subtitle	5. Report Date
MIXING OF SUPERSONIC JETS INCLUDING THE EFFECTS OF TRANSVERSE PRESSURE GRADIENT USING DIFFERENCE METHODS	December 1971
	6. Performing Organization Code
7. Author(s)	8. Performing Organization Report No.
Anatole P. Kurkov	E-6386
	10. Work Unit No.
9. Performing Organization Name and Address	764-75
Lewis Research Center National Aeronautics and Space Administration Cleveland, Ohio 44135	11. Contract or Grant No.
	13. Type of Report and Period Covered
12. Sponsoring Agency Name and Address	Technical Note
National Aeronautics and Space Administration Washington, D.C. 20546	14. Sponsoring Agency Code

15. Supplementary Notes

16. Abstract

The usual boundary-layer equations describing the steady-state mixing of parallel jets are supplemented by the momentum equation in the direction normal to the flow. This allows detailed computation of the flow field in the mixing region and simultaneous computation of the outer inviscid flow. An explicit and an implicit finite difference schemes have been developed and applied in several illustrative examples. The examples include mixing of planar and axisymmetric supersonic jets of different composition with both matched and unmatched static pressures. Numerical results were compared with available experimental data obtained for the unmatched pressure case.

17. Key Words (Suggested by Author(s))	18. Distribution Statement
Supersonic jet mixing Supersonic jets Finite-difference equations	Unclassified - unlimited

19. Security Classif. (of this report)	20. Security Classif. (of this page)	21. No. of Pages	22. Price*
Unclassified	Unclassified	31	$3.00

* For sale by the National Technical Information Service, Springfield, Virginia 22151

MIXING OF SUPERSONIC JETS INCLUDING THE EFFECTS OF TRANSVERSE PRESSURE GRADIENT USING DIFFERENCE METHODS

by Anatole P. Kurkov

Lewis Research Center

SUMMARY

The usual boundary-layer equations describing the steady-state mixing of parallel jets are supplemented by the momentum equation in the direction normal to the flow. This allows detailed computation of the flow field in the mixing region and simultaneous computation of the outer inviscid flow.

An explicit and an implicit finite difference schemes have been developed and applied in several illustrative examples. The examples include mixing of planar and axisymmetric supersonic jets of different composition with both matched and unmatched static pressures. Numerical results were compared with available experimental data obtained for the unmatched-pressure case.

INTRODUCTION

Traditionally, jet mixing problems are solved using the boundary-layer equations. As a result, the transverse pressure field in the mixing region is assumed to be uniform. In the case of a supersonic combustor this assumption may not always be justified. Significant pressure gradients can be induced as a result of combustion, or they can be created at the injection port if the static pressures of the fuel and air are not matched. In such cases the transverse momentum equations must be considered.

Previously (refs. 1 and 2), a numerical solution that incorporates the effects of the transverse pressure gradient was achieved by splitting the governing equations into a set of essentially inviscid equations and a set of viscous boundary-layer equations. In the first set of equations, which was written in the characteristic coordinates, viscous terms were treated as a perturbation. At each point it was necessary to iterate between the two sets of equations to match the two flows.

In the present computational scheme, all equations are differenced in the same coordinate system and the variables associated with viscous and inviscid effects are determined simultaneously. Two finite-difference schemes, an explicit and an implicit, were developed and evaluated.

The computer program was written for the solution of free or confined supersonic jet mixing. Initially, at the origin, the jets were assumed to have uniform properties and the turbulent Prandtl and Schmidt numbers were assumed to be unity. Figure 1 shows the general configuration of the jets; geometry can be either planar or axisymmetric.

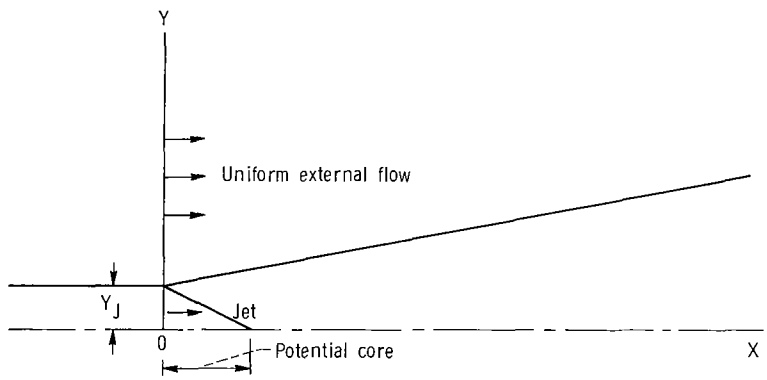

Figure 1. - Configuration of jet.

Computations have been carried out for planar free jet mixing of hydrogen at Mach 1.67, and air at Mach 2.5. Both, matched and unmatched pressure cases were considered. Additional cases were computed for the purpose of comparison with the theoretical and experimental results from the literature.

The computational scheme described in this report represents an alternate method to the usual scheme in which the inviscid and viscous flow fields are computed separately. However, in case of reacting jets, the later method can not predict accurately the effects of combustion on the flow field. Schemes such as the one described in this report must then be used. In case of purely inviscid flows the present finite-difference scheme, in comparison with the method of characteristics, is easier to apply to the computation of ducted flows that involve multiple reflections from the boundaries.

SYMBOLS

$\overline{A}$	matrix whose element are $a_{j,k}$ (eq. (31))
A_j	coefficient in eq. (24)
$a_{j,k}$	matrix element defined by eq. (32)
$\overline{B}$	vector whose elements are b_j (eq. (31))
B_j	coefficient in eq. (24)
b_j	vector element defined by eq. (35)
$b_{0.1}, b_{1/2}$	jet widths used in eddy viscosity expression, eqs. (36) and (37)
C_j	coefficient in eq. (24)
C_p	specific heat at constant pressure
c	speed of sound
D_j	defined by eq. (34)
d_j	defined by eq. (33)
E_j, F_j, G_j	defined by eqs. (29)
H	total enthalpy
h_k	static enthalpy
J	$J = 0$ for planar, and $J = 1$ for axisymmetric geometry
K	defined by eq. (21)
M	Mach number
n	coordinate normal to streamline
Δn	grid spacing in n direction
P	pressure
q	velocity
R	gas constant
R_0	universal gas constant
s	streamline coordinate
Δs	grid spacing in s direction
T	temperature
U	velocity component normal to the direction of the shock

U_j	defined by eqs. (29)
V_j	defined by eq. (16)
W_k	molecular weight for specie k
X, Y	rectangular Cartesian coordinates for planar configuration; axial and radial coordinates for axisymmetric configuration (see fig. 1)
Y_J	half-jet height or jet radius at origin
α_k	mass fraction for specie k
β	shock angle
γ	specific heat ratio
δ	boundary-layer thickness
ϵ	eddy (kinematic) viscosity; Mach angle, in the appendix
θ	flow angle
μ	turbulent viscosity
ρ	density

Subscripts:

C	centerline
E	external stream
J	central jet
k	refers to the particular specie; k = 1 for H_2, k = 2 for O_2, k = 3 for N_2

ANALYSIS

Basic Equations

In the equations, the account of the turbulence is accomplished by using eddy viscosity, which is assumed to be a function of local flow variables and local jet parameters. The variables in the equations are assumed to be time average quantities.

Starting with full equations of motion in streamline coordinates and proceeding with boundary-layer simplifications, it is possible to derive

$$\rho q \frac{\partial q}{\partial s} = - \frac{\partial P}{\partial s} + \frac{\partial}{\partial n}\left(\mu \frac{\partial q}{\partial n}\right) + J \frac{\mu \cos \theta}{Y} \frac{\partial q}{\partial n} \tag{1}$$

$$\rho q^2 \frac{\partial \theta}{\partial s} = -\frac{\partial P}{\partial n} + \frac{4}{3}\frac{\partial}{\partial n}\left(\mu q \frac{\partial \theta}{\partial n}\right) + \mu \frac{\partial q}{\partial n}\frac{\partial \theta}{\partial n} + \frac{\partial}{\partial s}\left(\mu \frac{\partial q}{\partial n}\right) - \frac{2}{3}\frac{\partial}{\partial n}\left(\mu \frac{\partial q}{\partial s}\right)$$

$$+ J\left\{\frac{\mu}{Y}\left[\frac{\partial q}{\partial n}\sin\theta + 2q\cos\theta\left(\frac{\partial \theta}{\partial n} - \frac{\sin\theta}{Y}\right)\right] - \frac{2}{3}\frac{\partial}{\partial n}\left(\mu \frac{q}{Y}\sin\theta\right)\right\} \tag{2}$$

where only the zero- and first-order terms were retained. In the equations (1) and (2), the turbulent viscosity is denoted by μ; P, q, θ, and ρ denote pressure, velocity, flow angle measured from X axis, and density; s and n are streamline and the normal-to-the-streamline coordinates; Y is the radial distance from the axis; and J = 0 or 1, depending on whether the flow is planar or axisymmetric. The first equation is the same as the usual boundary-layer equation. Considering the terms in this equation to be of zero order, all terms in the second equation are of the first order. Simultaneous solution of these equations would yield the solution accurate to the first order. However, the viscous terms in the second equation were found to affect the numerical solution in both the inviscid flow field and the mixing region only to a small degree. Omitting, therefore, the viscous terms in the second equation reduces it to

$$\rho q^2 \frac{\partial \theta}{\partial s} + \frac{\partial P}{\partial n} = 0 \tag{3}$$

Although the simultaneous solution of the equations (1) and (3) throughout the flow field does not produce now a uniformly valid first-order solution, it correctly predicts the inviscid part of the flow. Consequently, the viscous region does not have to be necessarily small compared with the inviscid region; also the problem of matching of the two regions is eliminated.

Assuming that the turbulent Prandtl and Schmidt numbers are equal to one, the energy and specie conservation equations are

$$\frac{\partial H}{\partial s} = \frac{1}{\rho q}\frac{\partial}{\partial n}\left(\mu \frac{\partial H}{\partial n}\right) + \frac{J}{\rho q}\mu \frac{\cos\theta}{Y}\frac{\partial H}{\partial n} \tag{4}$$

$$\frac{\partial \alpha_k}{\partial s} = \frac{1}{\rho q}\frac{\partial}{\partial n}\left(\mu \frac{\partial \alpha_k}{\partial n}\right) + \frac{J}{\rho q}\mu \frac{\cos\theta}{Y}\frac{\partial \alpha_k}{\partial n} \qquad k = 1, \ldots, N \tag{5}$$

where H is the total enthalpy, $H = \sum h_k \alpha_k + q^2/2$, and h_k and α_k are the specie enthalpy and mass fraction. The continuity equation is given by

$$q\frac{\partial \rho}{\partial s} + \rho\frac{\partial q}{\partial s} + \rho q\frac{\partial \theta}{\partial n} + J\frac{\rho q}{Y}\sin\theta = 0 \tag{6}$$

Denoting the temperature by T, universal gas constant by R_0, and the specie molecular weight by W_k, the equation of state is given by

$$P = \rho T R_0 \sum \frac{\alpha_k}{W_k} \tag{7}$$

It is possible to combine (ref. 3) the momentum equation (1), the continuity equation (6), and the equation of state (7) to obtain

$$\frac{1}{\rho q^2}\left(\frac{q^2}{c^2} - 1\right)\frac{\partial P}{\partial s} + \frac{\partial \theta}{\partial n} = \frac{1}{C_p T}\left\{\frac{\partial H}{\partial s} - \sum h_k \frac{\partial \alpha_k}{\partial s} - \left(q + \frac{C_p T}{q}\right)\frac{1}{\rho q}\left[\frac{\partial}{\partial n}\left(\mu\frac{\partial q}{\partial n}\right) + J\frac{\mu\cos\theta}{Y}\frac{\partial q}{\partial n}\right]\right\}$$

$$+ \frac{R_0}{R}\sum \frac{1}{W_k}\frac{\partial \alpha_k}{\partial s} - J\frac{\sin\theta}{Y} \tag{8}$$

where the specific heat C_p, the gas constant R, and the velocity of sound c are defined by

$$C_p = \sum \alpha_k \frac{dh_k}{dT} = \sum \alpha_k \left(C_p\right)_k \tag{9}$$

$$R = R_0 \sum \frac{\alpha_k}{W_k} \tag{10}$$

$$c = \left(\frac{C_p}{C_p - R} RT\right)^{1/2} \tag{11}$$

Ignoring for the moment the terms on the right side of equation (8), it is seen that when the flow is supersonic, this equation together with equation (3) constitute a typical hyperbolic system. The terms on the right in equation (8), with the exception of the last, arise because of viscous diffusion. These terms originate from purely parabolic conservation equations (1), (4), and (5). It is, therefore, seen that the equations are of mixed hyperbolic-parabolic character.

The Explicit Method

The difference equations for the parabolic equations (4) and (5) are obtained in the usual way. Written for the point (i, j) corresponding to the i^{th} interval in s direction and j^{th} interval in the n direction they are

$$\frac{H_{i+1,j} - H_{i,j}}{\Delta s_{i,j}} = \frac{1}{\rho_{i,j} q_{i,j}} \frac{\mu_i}{\Delta n_{i,j-1/2}} \left(\frac{H_{i,j+1} - H_{i,j}}{\Delta n_{i,j}} - \frac{H_{i,j} - H_{i,j-1}}{\Delta n_{i,j-1}} \right)$$

$$+ \frac{J}{\rho_{i,j} q_{i,j}} \frac{\mu_i \cos \theta_{i,j}}{Y_{i,j}} \frac{H_{i,j+1} - H_{i,j-1}}{\Delta n_{i,j} + \Delta n_{i,j-1}} \qquad (12)$$

$$\frac{(\alpha_k)_{i+1,j} - (\alpha_k)_{i,j}}{\Delta s_{i,j}} = \frac{1}{\rho_{i,j} q_{i,j}} \frac{\mu_i}{\Delta n_{i,j-1/2}} \left[\frac{(\alpha_k)_{i,j+1} - (\alpha_k)_{i,j}}{\Delta n_{i,j}} - \frac{(\alpha_k)_{i,j} - (\alpha_k)_{i,j-1}}{\Delta n_{i,j-1}} \right]$$

$$+ \frac{J}{\rho_{i,j} q_{i,j}} \frac{\mu_i \cos \theta_{i,j}}{Y_{i,j}} \frac{(\alpha_k)_{i,j+1} - (\alpha_k)_{i,j-1}}{\Delta n_{i,j} + \Delta n_{i,j-1}} \qquad (13)$$

where $\Delta s_{i,j}$ and $\Delta n_{i,j}$ denote the step sizes in the streamline and the normal directions (fig. 2). In these equations viscosity is assumed to depend only on streamline coordinate.

For the derivatives of P and θ associated with the hyperbolic-type left sides of equations (8) and (3) a typical hyperbolic difference scheme (ref. 4, p. 262) is used:

$$\frac{1}{\rho_{i,j} q_{i,j}^2} \left(\frac{q_{i,j}^2}{c_{i,j}^2} - 1 \right) \frac{P_{i+1,j} - P_{i,j}}{\Delta s_{i,j}} + \frac{\theta_{i,j+1/2} - \theta_{i,j-1/2}}{\Delta n_{i,j-1/2}} = V_j \qquad (14)$$

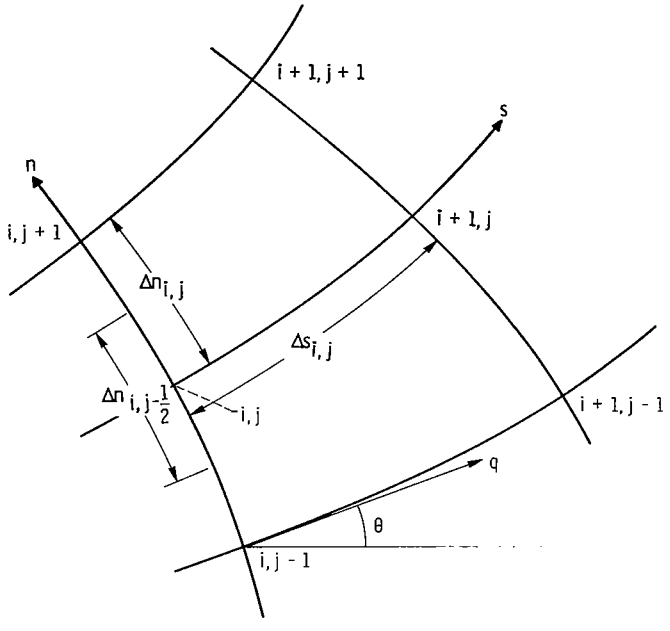

Figure 2. - Streamline coordinate system.

$$\rho_{i,j-1/2} q^2_{i,j-1/2} \frac{\theta_{i+1,j-1/2} - \theta_{i,j-1/2}}{\Delta s_{i,j-1/2}} + \frac{P_{i+1,j} - P_{i+1,j-1}}{\Delta n_{i,j-1}} = 0 \tag{15}$$

The term V_j denotes the differenced right side of equation (8),

$$V_j = \frac{1}{\left(C_p\right)_{i,j} T_{i,j}} \left\{ H'_{i,j} - \sum_k \left(h_k\right)_{i,j} \left(\alpha'_k\right)_{i,j} - \left[q_{i,j} + \frac{\left(C_p\right)_{i,j} T_{i,j}}{q_{i,j}} \right] \frac{1}{\rho_{i,j} q_{i,j}} \right.$$

$$\left. \left[\frac{\mu_i}{\Delta n_{i,j-1/2}} \left(\frac{q_{i,j+1} - q_{i,j}}{\Delta n_{i,j}} - \frac{q_{i,j} - q_{i,j-1}}{\Delta n_{i,j-1}} \right) + J \frac{\mu_i \cos \theta_{i,j}}{Y_{i,j}} \frac{q_{i,j+1} - q_{i,j-1}}{\Delta n_{i,j} + \Delta n_{i,j-1}} \right] \right\}$$

$$+ \frac{R_0}{R_{i,j}} \sum_k \frac{\left(\alpha'_k\right)_{i,j}}{W_k} - J \frac{\sin \theta_{i,j}}{Y_{i,j}} \tag{16}$$

where H' and α' denote differenced streamline derivatives of H and α given by equations (12) and (13). It is seen that θ is computed from equations (14) and (15) midway between the grid points; other variables are computed at the grid points. For the purpose of the computation of coefficients in the difference equations, values of θ at the grid points, as well as the values of other variables between the grid points, are obtained by linear interpolation.

In the axisymmetric case the two terms in equation (16) involving division by y become on the axis

$$\frac{\mu_i \cos \theta_{i,j}}{Y_{i,j}} \frac{q_{i,j+1} - q_{i,j-1}}{\Delta n_{i,j} + \Delta n_{i,j-1}} = \frac{\mu_i \cos \theta_{i,j}}{\Delta n_{i,j-1/2}} \left(\frac{q_{i,j+1} - q_{i,j}}{\Delta n_{i,j}} - \frac{q_{i,j} - q_{i,j-1}}{\Delta n_{i,j-1}} \right) \tag{17}$$

$$\frac{\sin \theta_{i,j}}{Y_{i,j}} = \frac{\theta_{i,j+1/2} - \theta_{i,j-1/2}}{\Delta n_{i,j-1/2}} \tag{18}$$

The last terms in equations (12) and (13) transform on the axis similarly, with q being replaced, respectively, by H and α. On the axis, also, normal derivatives must vanish so that

$$\begin{aligned} H_{i+1,j-1} &= H_{i+1,j+1} \\ \left(\alpha_k\right)_{i+1,j-1} &= \left(\alpha_k\right)_{i+1,j+1} \\ q_{i+1,j-1} &= q_{i+1,j+1} \end{aligned} \tag{19}$$

and, since the flow angle is zero,

$$\theta_{i+1,j+1/2} = -\theta_{i+1,j-1/2} \tag{20}$$

Conditions (19) and (20) also hold for the center plane in the planar case.

The outer boundary of the jet is assumed to be reached when the deviation from the uniform external flow is sufficiently small. As the jet expands, additional points in the normal direction are included in the grid. The outermost streamline is assumed to be undisturbed flow. At each step, the equations are solved in the following sequence: (12), (13), (16), (14), and (15). After each advance in the streamline direction, the Δs and Δn are incremented using simple geometry. For example,

$$\Delta n_{i+1,j-1/2} = \Delta n_{i,j-1/2} + \Delta s_{i,j}\left(\theta_{i,j+1/2} - \theta_{i,j-1/2}\right)$$

The equations being explicit there are two necessary stability criteria to be satisfied. One is associated with parabolic equations and one with the inviscid hyperbolic parts of equations (14) and (15) (ref. 4):

$$\Delta s_{i,j} < K\frac{\rho_{i,j}q_{i,j}}{\mu_i}\Delta n_{i,j}^2 \qquad K = \frac{1}{2} \tag{21}$$

$$\Delta s_{i,j} < \sqrt{M_{i,j}^2 - 1}\,\Delta n_{i,j} \tag{22}$$

where M is Mach number. In practice, in some cases, criterion (21) was not sufficient. A more stringent requirement was then imposed, $1/4 > K \geq 1/8$.

The Implicit Method

The difference equations are transformed into implicit form by expressing the derivatives in the normal direction in terms of variables evaluated at the advanced distance s. Thus, equation (12) becomes

$$\frac{H_{i+1,j} - H_{i,j}}{\Delta s_{i,j}} = \frac{1}{\rho_{i,j}q_{i,j}}\frac{\mu_i}{\Delta n_{i,j-1/2}}\left(\frac{H_{i+1,j+1} - H_{i+1,j}}{\Delta n_{i,j}} - \frac{H_{i+1,j} - H_{i+1,j-1}}{\Delta n_{i,j-1}}\right)$$

$$+ \frac{J}{\rho_{i,j}q_{i,j}}\frac{\mu_i \cos\theta_{i,j}}{Y_{i,j}}\frac{H_{i+1,j+1} - H_{i+1,j-1}}{\Delta n_{i,j} + \Delta n_{i,j-1}} \tag{23}$$

where, as in the explicit method, μ is assumed to depend only on the streamline coordinate. This leads to a tridiagonal system of equations:

$$-A_jH_{i+1,j-1} + B_jH_{i+1,j} - C_jH_{i+1,j+1} = \rho_{i,j}q_{i,j}H_{i,j} \tag{24}$$

where

$$A_j = \mu_i\,\Delta s_{i,j}\left[\frac{1}{\Delta n_{i,j-1/2}\,\Delta n_{i,j-1}} - \frac{\cos\theta_{i,j}}{Y_{i,j}\left(\Delta n_{i,j-1} + \Delta n_{i,j}\right)}\right] \tag{24a}$$

$$C_j = \mu_i \, \Delta s_{i,j} \left[\frac{1}{\Delta n_{i,j-1/2} \, \Delta n_{i,j}} + \frac{\cos \theta_{i,j}}{Y_{i,j} \left(\Delta n_{i,j-1} + \Delta n_{i,j} \right)} \right] \tag{24b}$$

$$B_j = \rho_{i,j} q_{i,j} + A_j + C_j \tag{24c}$$

Another tridiagonal system results from the equations for α_k

$$- A_j \left(\alpha_k \right)_{i+1,j-1} + B_j \left(\alpha_k \right)_{i+1,j} - C_j \left(\alpha_k \right)_{i+1,j+1} = \rho_{i,j} q_{i,j} \left(\alpha_k \right)_{i,j} \tag{25}$$

For the solution of systems of equations (24) and (25) there exists a simple algorithm (ref. 5, p. 14).

Equation (14) now involves advanced values of θ and q:

$$\frac{1}{\rho_{i,j} q_{i,j}^2} \left(\frac{q_{i,j}^2}{c_{i,j}^2} - 1 \right) \frac{P_{i+1,j} - P_{i,j}}{\Delta s_{i,j}} + \frac{\theta_{i+1,j+1/2} - \theta_{i+1,j-1/2}}{\Delta n_{i,j-1/2}} = V_j \tag{26}$$

$$V_j = \frac{1}{\left(C_p \right)_{i,j} T_{i,j}} \left\{ H'_{i,j} - \sum_k \left(h_k \right)_{i,j} \left(\alpha'_k \right)_{i,j} - \left[q_{i,j} + \frac{\left(C_p \right)_{i,j} T_{i,j}}{q_{i,j}} \right] \frac{1}{\rho_{i,j} q_{i,j}} \right.$$

$$\left. \left[\frac{\mu_i}{\Delta n_{i,j-1/2}} \left(\frac{q_{i+1,j+1} - q_{i+1,j}}{\Delta n_{i,j}} - \frac{q_{i+1,j} - q_{i+1,j-1}}{\Delta n_{i,j-1}} \right) + J \frac{\mu_i \cos \theta_{i,j}}{Y_{i,j}} \frac{q_{i+1,j+1} - q_{i+1,j-1}}{\Delta n_{i,j} + \Delta n_{i,j-1}} \right] \right\}$$

$$+ \frac{R_0}{R_{i,j}} \sum_k \frac{\left(\alpha'_k \right)_{i,j}}{W_k} - J \frac{\sin \theta_{i,j}}{Y_{i,j}} \tag{27}$$

while equation (15) is unchanged. The differenced derivatives in the streamline direction H' and α'_k in the identity (27) are calculated from the solution of systems of equations (24) and (25).

It is possible to eliminate θ from equations (15) and (26) to obtain

$$E_j P_{i+1,j-1} + F_j P_{i+1,j} + G_j P_{i+1,j+1} = U_j - \left(\rho q^2 \right)_{i,j+1/2} V_j \, \Delta n_{i,j-1/2} \tag{28}$$

where

$$U_j = (\rho q^2)_{i,j+1/2}\left[(\theta_{i,j+1/2} - \theta_{i,j-1/2}) - \frac{(M^2_{i,j} - 1)}{(\rho q^2)_{i,j}}\frac{\Delta n_{i,j-1/2}}{\Delta s_{i,j}} P_{i,j}\right]$$

$$E_j = \frac{(\rho q^2)_{i,j+1/2}}{(\rho q^2)_{i,j-1/2}}\frac{\Delta s_{i,j-1/2}}{\Delta n_{i,j-1}}$$

$$F_j = -\left[\frac{\Delta s_{i,j+1/2}}{\Delta n_{i,j}} + \frac{(\rho q^2)_{i,j+1/2}}{(\rho q^2)_{i,j-1/2}}\frac{\Delta s_{i,j-1/2}}{\Delta n_{i,j-1}} + \frac{(M^2_{i,j} - 1)(\rho q^2)_{i,j+1/2}}{(\rho q^2)_{i,j}}\frac{\Delta n_{i,j-1/2}}{\Delta s_{i,j}}\right] \qquad (29)$$

$$G_j = \frac{\Delta s_{i,j+1/2}}{\Delta n_{i,j}}$$

The unknowns in equations (28) are P and q (which appears in V_j); however, P can be eliminated using the implicitly differenced form of momentum equation (1),

$$\rho_{i,j} q_{i,j}\frac{q_{i+1,j} - q_{i,j}}{\Delta s_{i,j}} = -\frac{P_{i+1,j} - P_{i,j}}{\Delta s_{i,j}} + \frac{\mu_i}{\Delta n_{i,j-1/2}}\left(\frac{q_{i+1,j+1} - q_{i+1,j}}{\Delta n_{i,j}} - \frac{q_{i+1,j} - q_{i+1,j-1}}{\Delta n_{i,j-1}}\right)$$

$$+ \frac{J\mu_i \cos\theta_{i,j}}{Y_{i,j}}\frac{q_{i+1,j+1} - q_{i+1,j-1}}{\Delta n_{i,j-1} + \Delta n_{i,j}} \qquad (30)$$

The result is a five-diagonal system of equations. In matrix notation it is

$$\overline{A}q = \overline{B} \qquad (31)$$

The elements of matrix $\overline{A}$, $a_{j,k}$ are zero except for $j - 2 \le k \le j + 2$:

$$
\left.
\begin{aligned}
a_{j,j-2} &= E_j A_{j-1} \\
a_{j,j-1} &= D_j A_j - E_j B_{j-1} \\
a_{j,j} &= E_j C_{j-1} - D_j B_j + G_j A_{j+1} - d_j \\
a_{j,j+1} &= D_j C_j - B_{j+1} G_j \\
a_{j,j+2} &= C_{j+1} G_j
\end{aligned}
\right\} \tag{32}
$$

where d_j is defined by

$$
d_j = \frac{\left(\rho q^2\right)_{i,j+1/2}}{q_{i,j}} \frac{\Delta n_{i,j-1/2}}{\Delta s_{i,j}} \frac{q_{i,j}^2 + \left(C_p\right)_{i,j} T_{i,j}}{\left(C_p\right)_{i,j} T_{i,j}} \tag{33}
$$

and

$$
D_j = F_j - \frac{d_j}{\rho_{i,j} q_{i,j}} \tag{34}
$$

The general term for vector $\overline{B}$, b_j is given by

$$
\begin{aligned}
b_j = U_j - \left(\rho q^2\right)_{i,j+1/2} \Delta n_{i,j-1/2} \Bigg\{ & \frac{1}{C_{p\,i,j} T_{i,j}} \left[H'_{i,j} - \sum_k \left(h_k\right)_{i,j} \left(\alpha'_k\right)_{i,j} \right] \\
& + \frac{R_0}{R_{i,j}} \sum_k \frac{\left(\alpha'_k\right)_{i,j}}{W_k} - J \frac{\sin \theta_{i,j}}{Y_{i,j}} \Bigg\} - E_j \left[P_{i,j-1} + \left(\rho q^2\right)_{i,j-1} \right] \\
& - F_j \left[P_{i,j} + \left(\rho q^2\right)_{i,j} \right] - G_j \left[P_{i,j+1} + \left(\rho q^2\right)_{i,j+1} \right]
\end{aligned} \tag{35}
$$

Denoting the lower boundary streamline by j_F and the outer boundary streamline by j_L, it can be seen from equations (32) and (35) that elements $a_{j,k}$ and b_j must be modified for $j \leq j_F + 2$ and $j \geq j_L - 2$ in order to satisfy proper boundary conditions. At the outer boundary they are evaluated assuming that the flow variables for $j > j_L$ are equal to the free-stream values. The j_L is chosen so that the flow disturbance relative to the free stream is small.

The treatment of the lower boundary is the same for distances X that are less than the potential core length. Beyond the potential core, identities (17) and (18) must be used on the axis, with q evaluated at the advanced level in (17). In both, axisymmetric and planar cases, the matrix coefficients near the center streamline are evaluated using equations (19) and (20). The system of equations (31) was solved using specialized Gauss elimination method.

RESULTS AND DISCUSSION

Illustrative Examples

The results were obtained for free, two-dimensional jet mixing with both matched and unmatched pressures and for two different turbulent viscosity models. At the origin both jets were assumed to have uniform properties. The center jet was hydrogen with $P = 1.01\times10^5$ or 3.03×10^5 newtons per square meter, $M = 1.67$, $q = 2220$ meters per second, and $T = 306$ K. The external stream was air with $P = 1.01\times10^5$ newtons per square meter, $M = 2.48$, $q = 1630$ meters per second, and $T = 1110$ K. The two turbulent viscosities considered were constant viscosity and a more realistic formulation based on Prandtl kinematic eddy viscosity model (ref. 6, pp. 599 and 607):

$$\epsilon = 0.014\, b_{0.1} \left| q_E - q_J \right| + 0.0014 \tag{36}$$

for X less than the length of potential core, and

$$\epsilon = 0.037\, b_{1/2} \left| q_E - q_C \right| \tag{37}$$

for X greater than the potential core length. In the equation (36) $b_{0.1}$ is the width of the mixing zone measured between points where $\left| \alpha_1 - \alpha_{1J} \right| = 0.1$ and $\left| \alpha_1 - \alpha_{1E} \right| = 0.1$. The mass fraction α_1 designates the component originally constituting the jet (hydrogen). This definition of $b_{0.1}$ differs somewhat from one given in reference 6 where $b_{0.1}$ is defined using the velocity difference. Mass-fraction difference was cho-

sen here because the change in composition is clearly related to viscous effects, whereas the change in velocity may be due to inviscid effects. The width $b_{1/2}$ is measured between the jet centerline and the point where $|q - q_C| = 1/2 |q_E - q_C|$.

The value chosen for the constant viscosity case was $\mu = 4.79 \times 10^{-3}$ newtons-seconds per square meter, which is of the order of magnitude found in the fully developed turbulent jets.

The results were obtained for three cases. In case I the pressures were matched and the viscosity was constant. Case II was calculated with hydrogen pressure three times the external stream pressure while, as in the first case, viscosity was constant. In case III pressures were matched and eddy viscosity was calculated from equations (36) and (37).

Figure 3 presents pressure profiles at downstream distances $X/Y_J = 0.2$ (fig. 3(a));

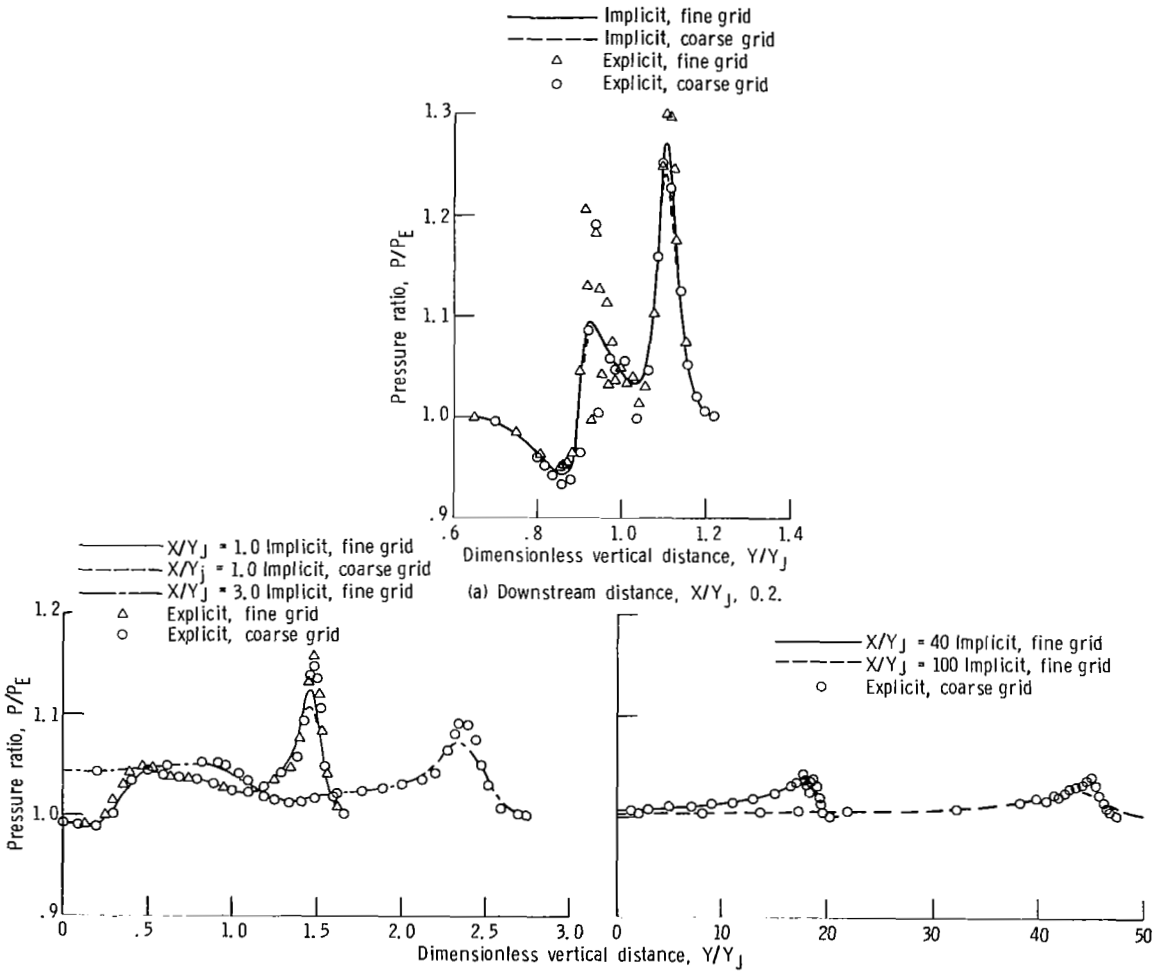

(a) Downstream distance, X/Y_J, 0.2.

(b) Downstream distance, X/Y_J, 1.0 and 3.0.

(c) Downstream distance, X/Y_J, 40 and 100.

Figure 3. - Pressure profile for constant viscosity. Initial pressure ratio, P_J/P_E, 1.

$X/Y_J = 1$ and 3 (fig. 3(b)); $X/Y_J = 40$ and 100 (fig. 3(c)). The half-jet height Y_J was assumed to be 0.1905 centimeter. Since the pressures were matched initially, the pressure waves noted in these figures are due to mixing. Close to the injector (fig. 3(a)), the pressure waves are steep; however, further downstream the wave amplitudes are progressively attenuated (figs. 3(b) and (c)).

In figure 3 comparison was also made between implicit and explicit solutions, with the degree of convergence indicated in figures 3(a) and (b) by presenting results computed for two grid sizes. It is seen that the convergence of the implicit method is good except in the narrow regions around the pressure peaks. The fine grid spacing was half the value of the coarse grid spacing in both implicit and explicit solutions. Decreasing the grid spacing further was considered impractical. The actual mesh size was varied during the calculation; however, past the initial portion, the number of points in the normal direction was limited to 90 for coarse grid and to 180 for fine grid. The explicit solution at $X/Y_J = 0.2$ (fig. 3(a)) is quite irregular with oscillatory behavior in the hydrogen region ($Y/Y_J < 1$). In this region no particular improvement could be noted by using a finer grid. However, further downstream, as the disturbed region propagates, the explicit solution approaches a smooth curve. Using this method, the resolution of the steep pressure wave in the air region is furthermore seen to be superior to the resolution obtained using the implicit method. At a distance of $X/Y_J = 100$ (fig. 3(c)) the difference between the explicit and implicit solutions appears to be significant on a relative basis although the absolute magnitude of the pressure wave at this distance is small. The agreement in the wave speed, however, is very good.

Another indication of the accuracy of the implicit method is presented in the next section where it is applied to the calculation of the inviscid flow field and compared with the method of characteristics.

The oscillatory behavior in the explicit solution was observed whenever criteria (21) required that $\Delta s \ll \Delta n$. This is usually the case in the region close to the injector exit where Δn must be small so that steep pressure waves could be resolved. The oscillation was also observed in the implicit solution when $\Delta s \ll \Delta n$. In this case, however, there is no restriction on Δs so that in figure 3 and in the following figures Δs was chosen equal to Δn.

Figure 4 presents profiles of hydrogen mass fraction for several downstream distances. It is seen that the implicit solution follows the explicit closely and that there is only a small difference between these and the solution obtained using conventional boundary-layer equations (P held constant). It is noted that the mixing zone is considerably narrower than the width of the pressure field.

The results for case II, when the jet pressure is three times that of the external flow, are shown in figures 5 and 6. The mixing region assumes a pressure somewhat below the average, with the expansion wave moving in the direction of the central jet and

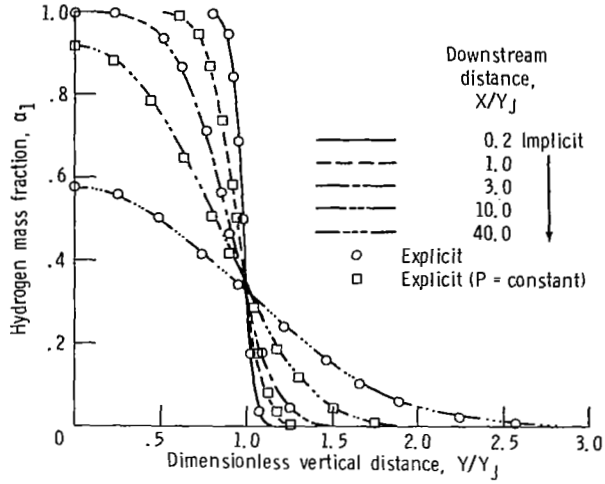

Figure 4. - Profiles of hydrogen mass fraction constant viscosity. Initial pressure ratio, P_J/P_E, 1.

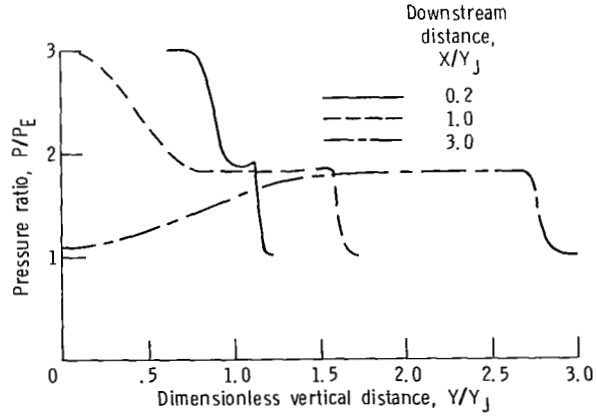

Figure 5. - Pressure profiles. Constant viscosity. Initial pressure ratio, P_J/P_E, 3.

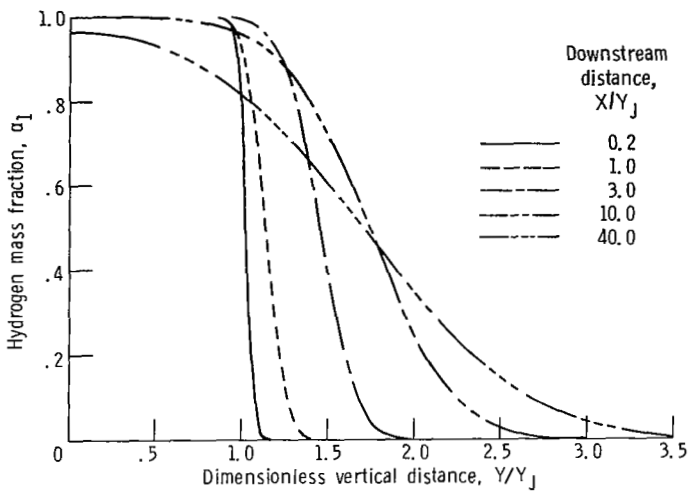

Figure 6. - Profiles of hydrogen mass fraction. Constant viscosity. Initial pressure ratio, P_J/P_E, 3.

the compression wave moving in the opposite direction. In figure 6 the mixing region is displaced considerably in the direction of the lower pressure external flow.

Figures 7 and 8 were obtained using equations (36) and (37) for the eddy viscosity. Physically, this represents a more realistic assumption and is typical of a number of available models that attempt to correlate experimental results. The amplitude of the pressure waves is much smaller in this case, although, a mild and fairly uniform pressure increase can be noted at $X/Y_J = 3$. It is evident that the near pressure field is very strongly dependent on the magnitude of the viscosity.

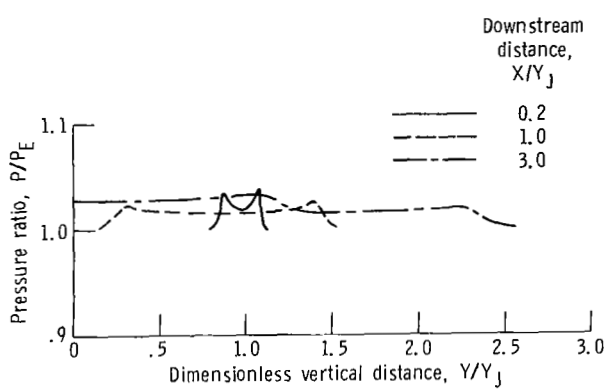

Figure 7. - Pressure profiles. Prandtl viscosity. Initial pressure ratio, P_J/P_E, 1.

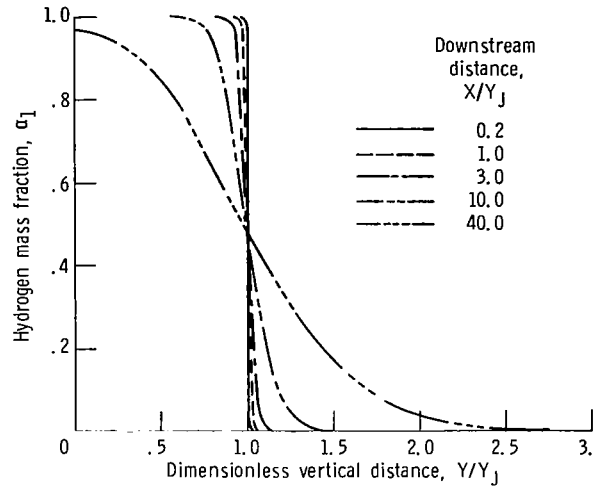

Figure 8. - Profiles of hydrogen mass fraction. Prandtl viscosity. Initial pressure ratio, P_J/P_E, 1.

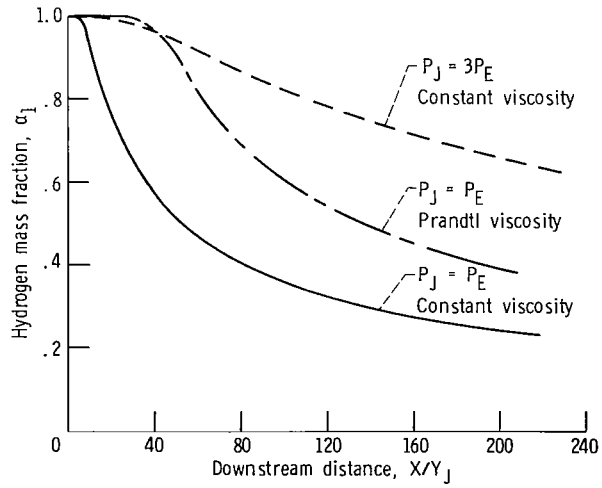

Figure 9. - Hydrogen mass-fraction distribution along center plane.

Figure 9 shows the distribution of hydrogen mass fraction along the center plane for all three cases. The potential core length for the Prandtl viscosity case is greater than that for the constant viscosity case due to smaller viscosity close to the injection point. The difference in the potential core length and in the rate of hydrogen concentration decay for the unbalanced pressure case is mainly due to the expansion of the hydrogen jet.

Figure 10 illustrates the positions of the mixing zones for cases I and II as determined by 1 and 99 percent hydrogen boundaries. Relative to the matched pressure case, the mixing zone in the unmatched pressure case is displaced in the direction of the lower pressure external flow.

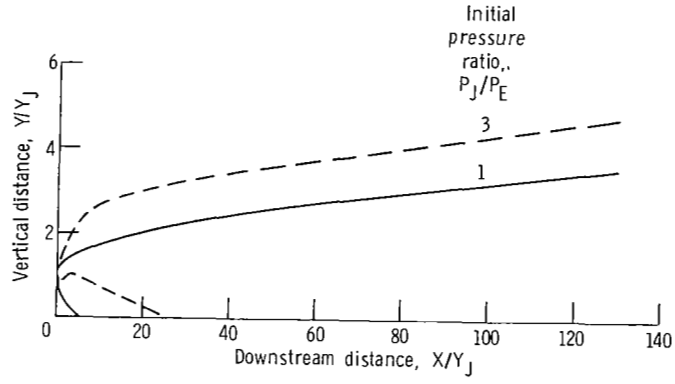

Figure 10. - 1 And 99 percent jet boundaries.

Comparison With the Literature

In figures 11 to 14 results were obtained for several axisymmetric jet mixing problems for the purpose of comparison with the numerical method of reference 1. Figure 11 presents pressure distribution along the centerline for free jet mixing assuming matched pressures and a constant turbulent viscosity. The present solution (explicit method) produces a much steeper pressure peak on the axis. A similar conclusion is reached from figure 12, which was obtained for underexpanded jet exhausting in a ducted coaxial flow assuming purely inviscid interaction. In this figure, the pressure peak at about $X/Y_J = 18$ is due to the reflection of the original compression wave from the upper wall. Included in the figure is the implicit solution computed for two grid sizes and also the solution obtained using the method of inviscid rotational characteristics presented in the appendix. It appears that a very fine mesh spacing is required for an accurate resolution of the pressure waves on the axis. There is still a noticeable departure of the fine-grid implicit solution from the points plotted for characteristics solution around the minimum pressure point in the first expansion wave. However, the difference between the char-

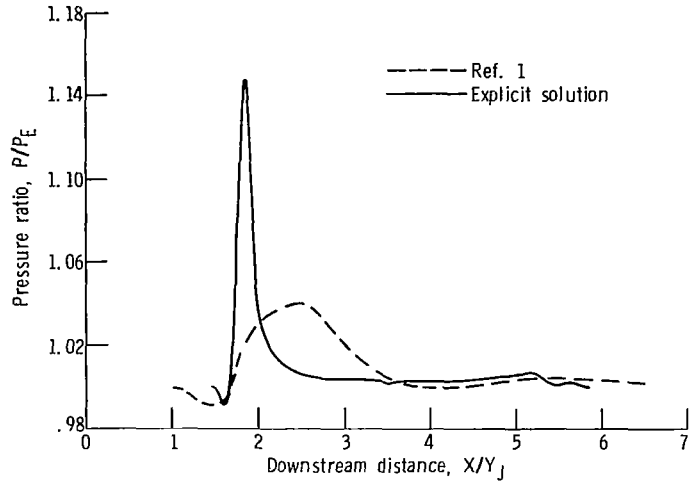

Figure 11. - Coaxial air jets, axial pressure distribution. Viscosity, 2.49×10^{-2} newton-second per square meter; jet radius, 2.5 centimeters. Initial properties of jet: pressure, 1.013×10^5 newtons per square meter; Mach 2; temperature, 1000 K. Initial properties of external flow: pressure, 1.013×10^5 newtons per square meter; Mach 3; temperature, 300 K.

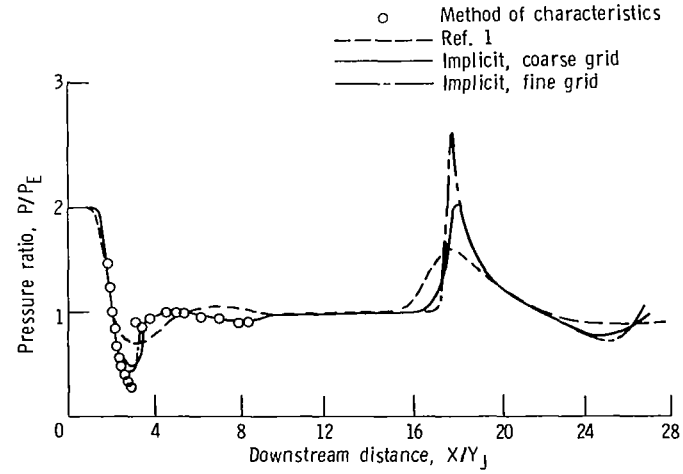

Figure 12. - Underexpanded ducted jet, centerline pressure distribution, inviscid case. Jet conditions: Mach 2.0; pressure, 5.06×10^5 newtons per square meter; temperature, 1100 K; gas, hygrogen; jet radius, 0.1 centimeter. External flow conditions: Mach 3.38; pressure, 2.533 newtons per square meter; temperature, 1500 K; gas, air; duct radius, 0.376 centimeter.

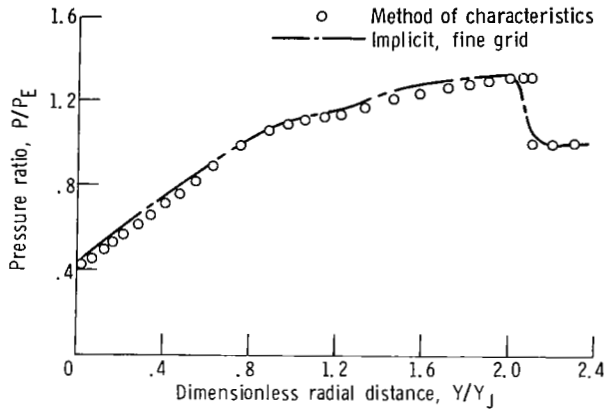

Figure 13. - Underexpanded ducted jet, pressure profile. Downstream distance, X/Y_J, 4.0; inviscid case.

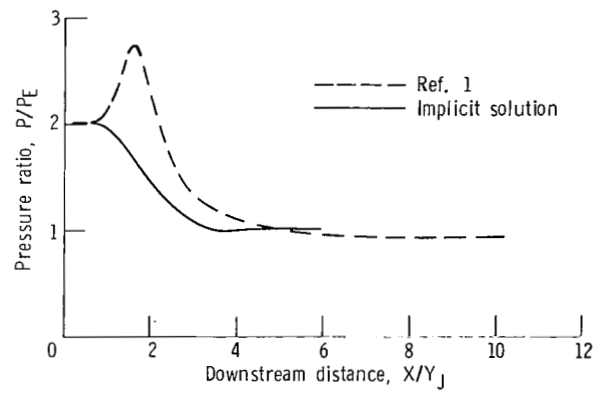

Figure 14. - Initial region of underexpanded ducted jet. Centerline pressure distribution; viscosity, 2.15×10^{-2} newton-second per square meter.

acteristics solution and the results obtained in reference 1 is even more pronounced. Unfortunately, no information is given in this reference on the degree of convergence of the solution.

A further indication of the accuracy of the implicit solution can be obtained from figure 13 where the pressure distribution at $X/Y_J = 4.0$ is compared with the corresponding results computed using the method of characteristics. It is seen that implicit method tends to smooth out the discontinuous compression wave at the outer boundary of the disturbed region. Similar tendency was noticed earlier in the discussion where implicit and explicit methods were compared.

Additional comparison with results from reference 1 is made in figure 14 which presents the centerline pressure distribution in the initial region of underexpanded jet in a ducted flow assuming a constant viscosity. It is difficult to explain the pressure rise at

$X/Y_J = 1.6$, noted in the solution of reference 1 even when considering (in view of results in fig. 12) that the grid spacing for this case was perhaps too coarse. Despite such poor agreement with reference 1 in figure 14, relatively small difference (about 10 percent for the range of X/Y_J covered in the figure) was observed comparing the hydrogen mass-fraction distributions on the centerline.

Comparison With the Experiment

In this section, the experimental results from a recent study of wall slot injection into a supersonic air stream (ref. 7) are compared with the finite-difference solution. A sketch of the wall slot is presented in figure 15. Also shown in this figure is the gen-

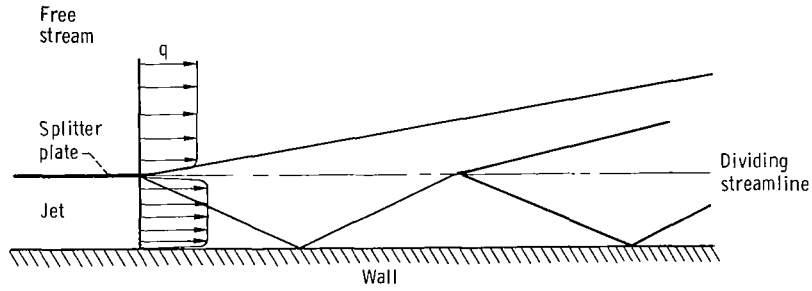

Figure 15. - Wall slot jet. Slot height, 1.27 centimeters; lip thickness, 0.0127 centimeters.

eral wave pattern and the extent of the boundary layer above the splitter plate for the particular series of experiments. The bottom-wall boundary layer was small compared with the slot height, and it did not seem to affect appreciably the wave pattern. In these experiments the composition of the jet was air, as was the composition of the free stream. The jet was supersonic with $M = 1.98$ and total temperature 297 K. In the free stream the total pressure and temperature were ambient with $M = 4.19$.

In the finite difference solution, viscosity was assumed to be given by

$$\mu = \rho\epsilon + \mu'$$

where μ' was taken to be of the order of molecular viscosity, $\mu' = 0.744 \times 10^{-5}$ newtons-seconds per square meter. The eddy viscosity ϵ was assumed to be given by equations (36) and (37) with the constant in equation (36) deleted and $b_{0.1}$ increased by adding a constant equal to the boundary-layer thickness. The computation was also carried out taking $\epsilon = 0$ and, consequently, $\mu = \mu'$; however, the difference was very small. The

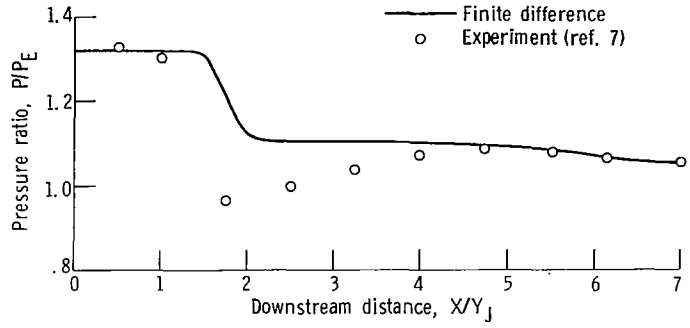

(a) Initial pressure ratio, P_J/P_E, 1.31.

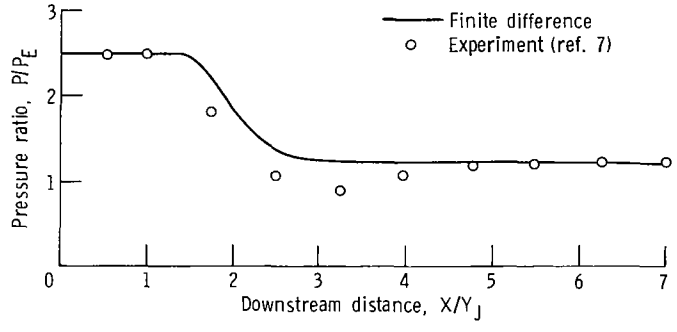

(b) Initial pressure ratio, P_J/P_E, 2.5.

Figure 16. - Pressure distribution on bottom wall, initially uniform external flow.

boundary layer on the bottom wall was not included in the calculation, and in figures 16 and 17 neither was the boundary layer above the splitter plate.

Figure 16(a) presents the wall-pressure distribution for the under-expanded slot jet with $P_J/P_E = 1.31$ at the injection point. For $X/Y_J < 4.0$, the agreement with the experiment is not very good; however, further downstream the agreement is much better. At X/Y_J about 5.5, in both the theoretical and experimental results, there is evidence of a weak reflection of the expansion wave from the mixing zone.

Figure 16(b) presents the wall-static pressure distribution for a higher initial pressure ratio of the two jets, $P_J/P_E = 2.5$. The contours of the dividing streamline for this case are shown in figure 17 where the experimental points were estimated from the photographs of reference 7. The agreement with the experiment is somewhat better in this case.

In order to explain the over-expansion and the higher apparent wave speed observed in the experimental results in figure 16(a), the computation was carried out with the eddy viscosity increased considerably beyond the value originally assumed. With this large viscosity it was possible to match the experimental wave speed and to obtain qualitatively

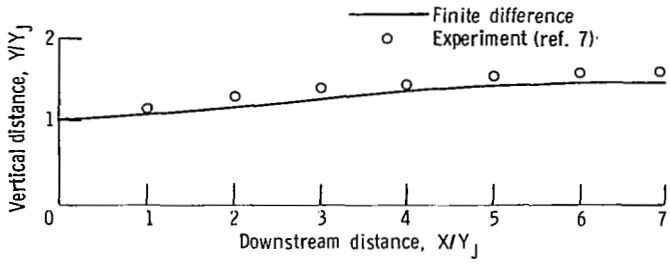

Figure 17. - Contour of dividing streamline, initially uniform external flow. Initial pressure ratio, P_J/P_E, 2.5.

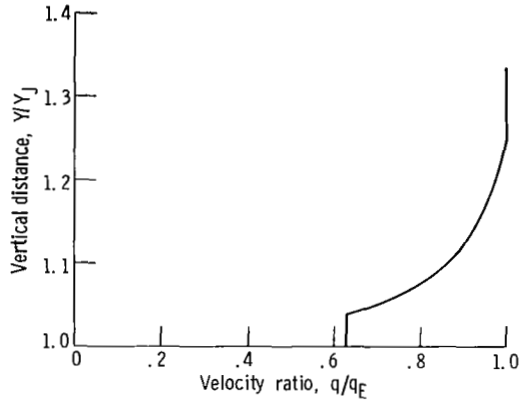

Figure 18. - Assumed velocity distribution in boundary layer.

similar pressure distribution. However, the mixing region in this case was much wider than indicated in the schlieren photographs of reference 7.

Next, the effect of the boundary layer above the splitter plate was investigated. It was assumed that density varies linearly in the boundary layer as given by

$$\rho = \rho_E \left(0.2 + 0.8 \frac{Y - Y_J}{\delta}\right)$$

which approximately matches the density variation in figure 44 of reference 7. To avoid the transonic and the subsonic regions in the boundary layer, uniform flow was assumed between the wall and the point where $M = 1.5$. The total enthalpy was assumed to be uniform throughout the boundary layer. The resulting velocity distribution in the boundary layer is shown in figure 18.

It can be seen in figure 19 that in this case the static pressure distribution more nearly approximates the experimental data. The apparent discrepancy in the wave speed

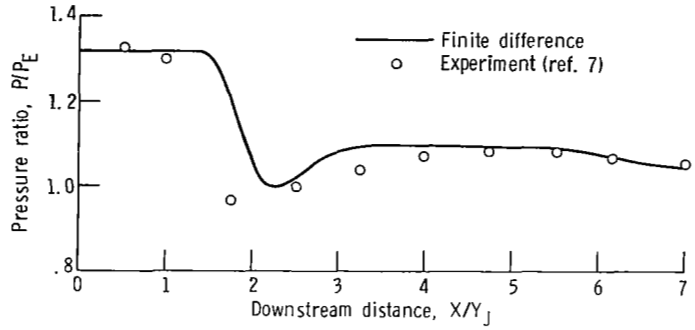

Figure 19. - Pressure distribution on bottom wall considering boundary layer in external flow. Initial pressure ratio, 1.31.

that is still present is probably due to the upstream propagation of the pressure disturbance on the bottom wall through the subsonic portion of the boundary layer.

CONCLUDING REMARKS

A numerical procedure has been developed for simultaneous computation of viscous and inviscid flow fields resulting from the supersonic mixing of jets.

The procedure can use either an explicit or an implicit finite difference scheme, each one having certain advantages and disadvantages. The explicit scheme sometimes produced an oscillatory solution. The oscillations were noticed in cases when the parabolic stability criterion requires that the streamwise grid spacing be much smaller than the spacing in the normal direction. The implicit scheme is generally free of this behavior; however, it is found that the resolution of the pressure waves generated as a result of mixing is not as good. The tendency is to smooth out the pressure gradients in the region where they are steep and, therefore, to reduce the magnitude of the pressure peaks. The mixing process, however, is found to be insensitive to the degree of accuracy with which the steep pressure variations are described. Illustrative examples comprise jet mixing with matched and unmatched static pressures. As a limiting case, the example for unmatched static pressures includes flow computation for purely inviscid jets. For this case, also, the method of inviscid rotational characteristics was used.

Lewis Research Center,
National Aeronautics and Space Administration,
Cleveland, Ohio, September 29, 1971,
764-75.

APPENDIX - METHOD OF CHARACTERISTICS FOR UNMATCHED-PRESSURE JETS

The inviscid rotational characteristics equations are derived in terms of variables P and θ from equations (3) and (8) in which the viscous terms are deleted. For rotational flows, working with these variables is more convenient than with usual variables q and θ or Prandtl-Meyer function and θ, which necessitate the introduction of another variable such as entropy.

Assuming that the data at mesh points 1 and 2 are known, the solution for point 3 is obtained from

$$Y_3 - Y_1 = (X_3 - X_1) \tan (\theta_1 - \epsilon) \tag{A1}$$

$$Y_3 - Y_2 = (X_3 - X_2) \tan (\theta_2 + \epsilon_2) \tag{A2}$$

$$\theta_1 - \theta_3 + \frac{\sin \epsilon_1 \cos \epsilon_1}{\gamma_1 P_1} (P_3 - P_1) + J \frac{\sin \epsilon_1 \sin \theta_1 (X_3 - X_1)}{\cos (\theta_1 - \epsilon_1) Y_1} = 0 \tag{A3}$$

$$\theta_3 - \theta_2 + \frac{\sin \epsilon_2 \cos \epsilon_2}{\gamma_2 P_2} (P_3 - P_2) + J \frac{\sin \epsilon_2 \sin \theta_2 (X_3 - X_2)}{\cos (\theta_2 + \epsilon_2) Y_2} = 0 \tag{A4}$$

where ϵ denotes the Mach angle and γ the specific heat ratio.

In the example in figures 12 and 13 the expansion of the central jet and the compression of the outer flow are determined so that the respective final pressures and final flow angles are the same. Since the gas is assumed to be calorically imperfect, the Prandtl-Meyer function for the expansion wave cannot be expressed as a function of Mach number only. It is more direct to solve the expansion wave by integrating θ first, since it can be expressed as a function of T only:

$$d\theta = \sqrt{\frac{2[H - h(T)]}{\gamma(T) R T} - 1} \frac{C_p(T)}{2[H - h(T)]} dT \tag{A5}$$

where for h(T) and $C_p(T)$ the same expressions were used as in the finite-difference program. In the expansion region pressure can also be expressed as a function of T by integrating

$$\frac{dP}{P} = \frac{C_p(T)}{RT} dT \tag{A6}$$

For the compression shock in the external stream it can be shown, using the conservation of mass and momentum in the direction normal to the shock and the equation of state, that the following equation must hold:

$$T_1 + \frac{U_1^2}{R} = \left(T_2 + \frac{U_2^2}{R}\right)\frac{U_1}{U_2} \tag{A7}$$

where 1 and 2 refer to the upstream and downstream sides of the shock and U denotes the component of q normal to the direction of the shock. Denoting the shock angle by β, U_1 and U_2 are given by

$$U_1 = \sqrt{2\left[H - h(T_1)\right]}\sin\beta \tag{A8}$$

and

$$U_2 = \sqrt{U_1^2 + 2\left[h(T_1) - h(T_2)\right]} \tag{A9}$$

In the computation scheme, initially β must be assumed. Using this value of β, T_2 is then iterated until equation (A7) is satisfied within acceptable limits. This allows calculation of θ_2 from

$$\sin(\beta - \theta_2) = \frac{U_2}{q_2} \tag{A10}$$

the density ρ_2 from the continuity equation across the shock,

$$\rho_1 U_1 = \rho_2 U_2 \tag{A11}$$

and P_2 from the equation of state,

$$P_2 = \rho_2 R T_2 \tag{A12}$$

In the expansion region, the integration of equation (A5) gives $\theta = \theta(T)$ in tabular form. The temperature at the end of expansion is obtained by interpolation from this table using $\theta = \theta_2$. Integration of equation (A6) gives now the pressure at the end of expansion. This pressure is compared with P_2. If the difference exceeds a prescribed tolerance, a new value of β is assumed, and the iteration is continued.

Downstream of the initial point the treatment of the shock differs to the extent that β is iterated until the compatibility condition (A4) is satisfied using θ and P determined from equations (A10) and (A12).

At the interface of the two jets, the pressure and flow angle must be the same on both sides, and they must also satisfy the compatibility equations: on the side of the outer stream, equation (A3); and on the jet side, equation (A4).

REFERENCES

1. Edelman, R.; and Weilerstein, G.: Mixing and Combustion in Supersonic Flow with Lateral Pressure Gradient Effects. Rep. GASL-TR-636, General Applied Science Labs., Inc. (NASA CR-97068), Aug. 1968.

2. Edelman, R. B.; and Weilerstein, G.: A Solution of the Inviscid-Viscid Equations with Applications to Bounded and Unbounded Multicomponent Reacting Flows. Paper 69-83, AIAA, Jan. 1969.

3. Moretti, Gino: Analysis of Two-Dimensional Problems of Supersonic Combustion Controlled by Mixing. Paper 64-96, AIAA, Jan. 1964.

4. Richtmyer, Robert D.; and Morton, K. W.: Difference Methods for Initial-Value Problems. Second ed., Interscience Publishers, 1967.

5. Douglas, J.: A Survey of Numerical Methods for Parabolic Differential Equations. Advances in Computers. Vol. 2. F.L. Alt, ed., Academic Press, 1961, pp. 1-54.

6. Schlichting, Hermann (J. Kestin, trans.): Boundary Layer Theory. Fourth ed., McGraw-Hill Book Co., Inc., 1960.

7. Schetz, Joseph A.; Gilreath, Harold E.; Waltrup, Paul J.; and Lewis, David P.: Research on Slot Injection into a Supersonic Air Stream. Rep. AERO-68-1, Maryland Univ. (AFAPL-TR-68-97, AD-839872), Sept. 1968.

NASA-Langley, 1971 —— 12 E-6386